Fatigue Fract. Engng Mater. Struct. Vol. 12, No. 2, pp. 105–122, 1989
Printed in Great Britain

8756-758X/89 $3.00 + 0.00
Fatigue of Engineering Materials Ltd

INFLUENCE OF SECONDARY VOID DAMAGE IN THE MATRIX MATERIAL AROUND VOIDS

G. C. LI
Institute of Mechanics, Academia Sinica, Beijing, China

and

T. GUENNOUNI and D. FRANÇOIS
Ecole Centrale, Paris, 92295 Chatenay-Malabry Cedex, France

(*Received in final form* 6 *June* 1988)

Abstract—The mechanism of ductile damage caused by secondary void damage in the matrix around primary voids is studied by large strain, finite element analysis. A cylinder embedding an initially spherical void, a plane stress cell with a circular void and plane strain cell with a cylindrical or a flat void are analysed under different loading conditions. Secondary voids of smaller scale size nucleate in the strain hardening matrix, according to the requirements of some stress/strain criteria. Their growth and coalescence, handled by the empty element technique, demonstrate distinct mechanisms of damage as circumstances change. The macroscopic stress–strain curves are decomposed and illustrated in the form of the deviatoric and the volumetric parts. Concerning the stress response and the void growth prediction, comparisons are made between the present numerical results and those of previous authors. It is shown that loading condition, void growth history and void shape effect incorporated with the interaction between two generations of voids should be accounted for besides the void volume fraction.

NOMENCLATURE

a = primary void radius
a_2 = the width of primary void in flat shape
L_1 = half-height along the major loading axis of the unit model
L_2 = half-width along the minor loading axis of the unit model
r = normalized initial radius or half-width of primary void ($=a_0/L_{20}$ or a_{20}/L_{20})
U_r = normalized radial displacement of the lateral boundary in cylinder model ($=\Delta L_2/L_{20}$)
W_z = normalized axial displacement at the end of cylinder model ($=\Delta L_1/L_{10}$)
U_x = normalized displacement along the major loading axis of the unit model ($=\Delta L_1/L_{10}$)
V_y = normalized displacement along the minor loading axis of the unit model ($=\Delta L_2/L_{20}$)
α = loading parameter that governs the overall strain ratio of the unit model
σ_e, ϵ_e = equivalent stress and strain in the deviatoric space
σ_m, ϵ_m = mean stress and strain in the volumetric space
E = Young's modulus
σ_y, ϵ_y = yield stress and strain
n = the exponent parameter in strain-hardening material that obeys the power law
t = generalized time
f_{v1} = the volume fraction of primary void
f_v = the total volume fraction of voids, including the primary and the secondary ones
$\tilde{\sigma}, \tilde{\epsilon}$ = overall stress, strain of the unit model
σ, ϵ = local stress, strain in the matrix material of the unit model
T = triaxiality parameter ($=\tilde{\sigma}_m/\tilde{\sigma}_e$)
suffix "0" denotes a variable at the initial time

1. INTRODUCTION

In search of a solution for the ductile fracture problem, many researchers have been focusing attention on void modelling, since the pioneering works of McClintock [1] and Rice and Tracey

[2]. Their results provided some simple formulas to estimate the void growth as a function of macroscopic stress and of macroscopic strain. As a consequence, the expansion of void volume results in an overall plastic dilatation. Gurson [3] developed approximate yield criteria and flow rules for porous (dilatant) rigid-plastic material, showing the role of triaxial tensile stress in plastic yield and the monotonous shrinking, or strain-softening effect, of this yield surface with respect to the increase of the porosity chosen. Guennouni and François [4] proposed a new plastic potential for porous rigid plastic material in plane strain conditions. They found that Gurson's model had overestimated the stress response of porous material in the rigid–plastic case, especially within the intermediate range of triaxial stress states. Guennouni and François [5] made use of their plastic potential to characterize the behaviour of the matrix material with secondary voids surrounding a relatively large cylindrical void in another plane strain model. They indicated the strong interaction between two orders of voids.

Application of the Gurson model to the shear band localization problem by Yamamoto [6] had shown that it did not necessarily seem to allow localization at reasonable strains unless some large value of porosity or initial imperfection within a thin slice of material should be considered. Tvergaard [7] had also experienced that the critical strain for localization into a shear band was considerably overestimated, when using the Gurson model. He then [8] claimed that much improvement could be obtained by a relatively simple modification of the equations suggested by Gurson.

Growing voids embedded in a strain-hardening matrix were treated in a more realistic way by employing the finite element method with large strain analysis. Needleman [9] made an elastic–plastic analysis of a plane strain cell, including both the geometrical nonlinearities resulting from large deformation and the physical nonlinearities arising from plastic material. Besides the works on plane strain models [7], Tvergaard also studied the macroscopic behaviour of axisymmetric cylinders including a growing void of initially spherical shape [8]. Li and Howard [10] proposed to use a strain-softening description, by assigning a negative value to the tangent modulus of the Prandtl–Reuss equation, when the local stress state in the matrix of the strain-hardening material reached a critical level. This strain-softening effect in the matrix was shown to have a substantial favouring effect on the growth of the initial void. Employing their model, Li and Howard [11] indicated the sensitivity of the macroscopic consequences of void growth to various mechanical and geometrical micro-parameters.

Physically speaking, usually there are at least two generations of voids in most engineering materials. The primary ones may nucleate around large inclusions ($\sim 10\ \mu$m) at an early stage of plastic deformation, whereas the secondary ones that have stronger bonding strength with smaller particles ($\sim 1\ \mu$m) of carbides or precipitates can only be debonded at rather high stress–strain levels. This microstructural process of ductile damage was observed in many experiments by different authors, such as Hancock and Mackenzie [12], Lautridou and Pineau [13], Sun *et al.* [14], Xia, Yang *et al.* [15] and Sun and François [16]. The texts of Hancock and Mackenzie [12] and of Lautridou and Pineau [13] had also shown the strong dependence of the ductility of material on the orientation of the inclusions, as for example, in the case of the long transverse and the short transverse samples. Sun *et al.* [14] and later on Marini *et al.* [17] indicated that the theoretical model of Rice and Tracey [2] had considerably underestimated the actual void growth observed in their tests.

The unanswered questions involved in the previous studies draw our attention on making further investigations on the ductile damage caused by secondary voids in the matrix material around primary voids. A wide range of loading conditions and of stress states was selected for the study, using axisymmetric, plane stress and plane strain models made of a strain-hardening material.

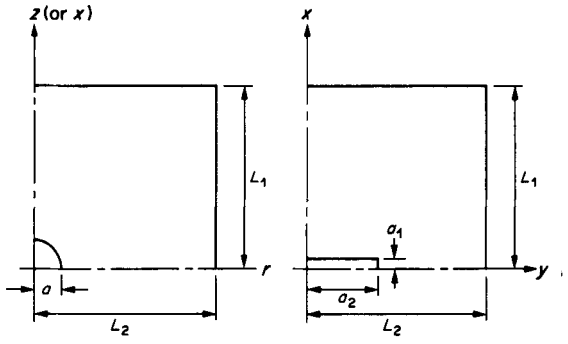

(a) Model with spherical or cylindrical void (b) Model A with flat void

Fig. 1. A quadrant model cell.

Secondary voids were assumed to be nucleated gradually, when a certain stress or strain criterion was met in the matrix, during the computations handled by a large strain finite element method. The sensitivity of the macroscopic consequences of void growth to various microstructural parameters and comparisons with the results of previous authors will be presented in the present paper.

2. MODEL CELL WITH TWO GENERATIONS OF VOIDS

It is shown in Fig. 1, a quadrant of the model cell that is to be analysed in axisymmetric, plane stress and plane strain loadings. The unit cell is taken from a porous material with primary voids that are assumed to be periodically distributed. Computations are made with three types of primary void shapes.

(a) Spherical one in an axisymmetric cylinder, the initial ratio of void radius a_0 and cylinder radius L_{20} being given as

$$r = a_0/L_{20} \tag{1}$$

in Fig. 1(a).

(b) Cylindrical one in plane stress or plane strain loadings with the parameters a_0 and L_{20} representing the initial radius of the void and the half-length along the minor loading axis of the unit in Fig. 1(a), respectively.

(c) Flat void in plane strain condition of Fig. 1(b) with its initial geometrical parameter as

$$r = a_{20}/L_{20}. \tag{2}$$

Here and hereafter we always use a suffix "0" to denote a variable at the initial time.

To simplify the computer simulation work, a proportional straining condition of loading is enforced at the boundary, rather than a more rigorous condition ensuring the continuity of both stress and displacement. Comparisons showed that this should not introduce too large discrepancies. Then the mechanical response of the cell is depending on the value of a parameter α which governs the overall strain ratio of the model. That is to say, during an incremental displacement loading

$$\frac{\mathrm{d}U_r}{L_2/L_{20}} = -\alpha \frac{\mathrm{d}W_z}{L_1/L_{10}} \quad \begin{pmatrix} W_2 = \Delta L_1/L_{10} \\ U_r = \Delta L_2/L_{20} \end{pmatrix} \tag{3}$$

in the axisymmetric case, and

$$\frac{dV_y}{L_2/L_{20}} = -\alpha \frac{dU_x}{L_1/L_{10}} \quad \begin{pmatrix} U_x = \Delta L_1/L_{10} \\ V_y = \Delta L_2/L_{20} \end{pmatrix} \tag{4}$$

for the plane stress or plane strain loading. In all the cases considered the initial geometrical aspect ratio of the model is taken as $L_{10}/L_{20} = 1$. Besides the incremental displacement condition assigned at the boundary, the shear stress along all the sides of the boundary is taken to be zero.

For all the examples calculated in this paper, the matrix material that surrounds the primary void is assumed to obey the power law in strain-hardening condition as

$$\left(\frac{\sigma_e}{\sigma_y}\right) = k\left(\frac{\epsilon_e}{\epsilon_y}\right)^n, \quad k = 1 \tag{5}$$

where σ_e, ϵ_e, σ_y and ϵ_y are the equivalent stress, the equivalent strain (neglecting the difference between the total one and the plastic part in large strain analysis), the yield stress ($=0.002\ E$, E is Young's modulus) and the yield strain ($=0.002$) of the matrix, respectively. The exponent parameter in (5) is chosen as $n = 0.15$, which can represent a series of high strength steels and the Poisson's ratio is taken as 0.3. Following the results of the tests [12–15], regarding the initiation of the secondary voids, we prefer to have a stress criterion

$$\sigma_m + \lambda\sigma_e = \sigma_c \tag{6}$$

or a strain criterion

$$\epsilon_e = \epsilon_c, \tag{7}$$

whichever is the first to be reached, throughout the following computations. In (6), σ_e and σ_m are the local equivalent stress and mean stress in the matrix, respectively, λ is a factor which is dependent on the shape of particles and is chosen to be 1.7 and σ_c is the critical stress that is taken as

$$\sigma_c = 7\sigma_y.$$

For the strain controlled nucleation, the critical value of the local equivalent strain ϵ_e is chosen as

$$\epsilon_c = 1.3.$$

The solution of the problem is obtained through the use of the up-dated Lagrangian formulation of McMeeking and Rice [18] with an appropriate generalization of the classical Prandtl–Reuss equations for the constitutive description of the matrix behaviour.

The quadrants in (a) and (b) of Fig. 1 are subdivided into 436 constant strain triangular elements with 248 nodal points and 438 elements with 250 points, respectively. In each of the element, once the stress–strain level attains either of the limiting conditions given by (6) and (7) it will be emptied, or in other words, it has no more stiffness. This empty element may then deform freely or coalesce with its neighbouring elements as loading proceeds. We take this process as the nucleation, growth and coalescence of the secondary voids. Since this event can actually take place at any site of the matrix, there is no point in choosing a finer mesh around the primary void than that for the other part of the matrix. We therefore decide to use an approximately equal size of triangular elements within the whole domain of matrix.

The elongation along the main loading axis is selected as the generalized time t. The method of computation within each increment Δt of time in the up-dated Lagrangian formulation of the

problem together with the generalized Prandtl–Reuss equations were explained by Li and Howard [10]. The number of the incremental steps needed to complete each calculation varies from 300 to 3000, depending on the ductility of the sample. Once the first secondary void initiates in the matrix, small incremental steps must be used for carrying on subsequent computations. This measure is taken to eliminate the computational error that could be caused by the local elastic unloading occurring suddenly around the newly nucleated void. Computations with a much finer mesh of equal size triangles (1209 elements, 654 nodes) had been employed to check the accuracy of the results obtained with the coarser mesh mentioned previously in regard to the macroscopic responses and the void growth. The calculations with these two meshes resulted in a difference less than 1% for both values of overall axial stress and the volume fractions of primary void, when that overall axial stress attained a maximum. The appropriate sizes of loading increments for each sample at different stages are also carefully handled and chosen to obtain convergent calculations.

3. MODELS UNDER DIFFERENT LOADING CONDITIONS

For the case of axisymmetric loading, a primary spherical void which has an initial radius ratio value of $r = 0.15$ is embedded in a cylinder and makes up an initial void volume fraction $f_{v0} = 0.225\%$. During proportional straining at the boundaries of this cylindrical cell shown in Fig. 1(a), the overall principal true strains can be related to the elongation W_z and the radial deformation U_r as

$$\bar{\epsilon}_z = \ln(1 + W_z)$$

$$\bar{\epsilon}_r = \ln(1 + U_r) = -\alpha\bar{\epsilon}_z.$$

From these we have for the overall equivalent strain and mean strain

$$\bar{\epsilon}_e = \tfrac{2}{3}(\bar{\epsilon}_z - \bar{\epsilon}_r)$$

and

$$\bar{\epsilon}_m = \frac{2\bar{\epsilon}_r + \bar{\epsilon}_z}{3}$$

respectively.

Let the average axial stress be $\bar{\sigma}_2$ and the average radial stress denoted as $\bar{\sigma}_r$, then, the overall equivalent stress and mean stress should respectively be

$$\bar{\sigma}_e = \bar{\sigma}_z - \bar{\sigma}_r$$

and

$$\bar{\sigma}_m = \frac{\bar{\sigma}_z + 2\bar{\sigma}_r}{3}.$$

Here and hereafter we use a bar on stress or strain to denote the macroscopic or overall response of the model. It is expected that such an axisymmetric model is more rigid than a 3 dimensional one.

In the plane stress model an initial circular void illustrated in Fig. 1(a) has a radius ratio $r = 0.15$ which corresponds to an initial void volume fraction $f_{v0} = 1.76\%$. During displacement controlled

loading the following relationships for the overall stresses and strains are employed.

$$d\bar{\epsilon}_x = dU_x/(1 + U_x)$$
$$d\bar{\epsilon}_y = dV_y/(1 + V_y) = -\alpha\, d\bar{\epsilon}_x$$
$$d\bar{\epsilon}_z = \int_A d\epsilon_z dA/A$$

here, $d\epsilon_z$ is the local strain along the z direction and A is the matrix area, so, $d\bar{\epsilon}_z$ means an average value over this area.

$$d\bar{\epsilon}_e = \frac{\sqrt{2}}{3}[(d\bar{\epsilon}_x - d\bar{\epsilon}_z)^2 + (d\bar{\epsilon}_y - d\bar{\epsilon}_z)^2 + (d\bar{\epsilon}_x - d\bar{\epsilon}_y)^2]^{1/2}$$

$$\bar{\epsilon}_e = \int_0^t d\bar{\epsilon}_e \quad d\bar{\epsilon}_m = (d\bar{\epsilon}_x + d\bar{\epsilon}_y + d\bar{\epsilon}_z)/3$$

$$\bar{\epsilon}_m = \int_0^t d\bar{\epsilon}_m \quad \bar{\sigma}_e = [\bar{\sigma}_x^2 - \bar{\sigma}_x\bar{\sigma}_y + \bar{\sigma}_y^2]^{1/2}$$
$$\bar{\sigma}_m = (\bar{\sigma}_x + \bar{\sigma}_y)/3$$

where $\bar{\sigma}_x$ and $\bar{\sigma}_y$ are the average stresses along the outer boundary lines.

As another typical loading we studied the plane strain model embedding a cylindrical void as shown in Fig. 1(a). Ratio values of $r = 0.15$ and 0.25 were chosen to account for the effect of initial void volume fractions f_{v0}, equal to 1.76 and 4.90%, respectively. A flat void shown in Fig. 1(b) will be employed to study the effect of void size in the next section.

In the present case we may find the following relations

$$\bar{\epsilon}_x = \ln(1 + U_x)$$
$$\bar{\epsilon}_y = \ln(1 + V_y) = -\alpha\bar{\epsilon}_x$$
$$\bar{\epsilon}_e = \tfrac{2}{3}(1 + \alpha + \alpha^2)^{1/2}\,\bar{\epsilon}_x$$
$$\bar{\epsilon}_m = (1 - \alpha)\,\bar{\epsilon}_x/3$$
$$\bar{\sigma}_e = \frac{1}{\sqrt{2}}[(\bar{\sigma}_x - \bar{\sigma}_y)^2 + (\bar{\sigma}_x - \bar{\sigma}_z)^2 + (\bar{\sigma}_y - \bar{\sigma}_z)^2]^{1/2}$$

and

$$\bar{\sigma}_m = (\bar{\sigma}_x + \bar{\sigma}_y + \bar{\sigma}_z)/3$$

where

$$\bar{\sigma}_z = \int_A \sigma_z dA/L_1L_2$$

and A is the matrix area, so, $\bar{\sigma}_z$ is an average value of the stress along the z direction.

The stress–strain curves calculated for $\alpha = 0.30$, 0.35, 0.40, 0.45, 0.47, 0.48 and 0.49 are illustrated in Fig. 2(a) for axisymmetric loading, where the total response is decomposed into a deviatoric part ($\bar{\sigma}_e$ vs $\bar{\epsilon}_e$) and a volumetric part ($\bar{\sigma}_m$ vs $\bar{\epsilon}_m$), with $r = 0$ representing the continuum behaviour of the matrix material which itself is incompressible in plasticity and has the volumetric strain contributed only by elasticity. The level of triaxiality is characterized by the parameter $T = \bar{\sigma}_m/\bar{\sigma}_e$ attained for each value of α. We may approximately refer the condition of $\alpha = 0.3$ to

the case of a material near to an existing crack. As the values of α increase to 0.49, triaxiality decreases gradually and approaches the condition of the material at the centre of an axisymmetrically notched bar and finally of a smooth bar. The point where the axial stress $\bar{\sigma}_z$ attains a maximum is marked by a short dash on the curves.

In Fig. 2(b) the results of the relationships of $\bar{\sigma}_e$ vs $\bar{\epsilon}_e$ and $\bar{\sigma}_m$ vs $\bar{\epsilon}_m$ for $\alpha = -1$, -0.6, -0.3, -0.1, 0, 0.1, 0.3, 0.45, 0.55 and 0.65 in plane stress conditions are depicted. Comparing with the axisymmetric case we find the triaxial tension is here much lowered down. Another salient feature is that the ductility does not vary monotonously as previously with the enhancement of the triaxial stress. It actually has the lowest value at $\alpha = 0$, which is a plane strain condition. From which either an increase or a decrease of the general mean stress enhances the ductility. This situation seems to be quite similar to the general trend resulting from metal sheet forming.

Macroscopic stress–strain curves for $r = 0.15$ are represented by solid lines in Fig. 2(c) for plane strain loading with $\alpha = -1$, -0.6, -0.3, 0, 0.3, 0.45, 0.55, 0.65, 0.75, 0.85 and $\sigma_y = 0$. The ductility is now again varying monotonously with the degree of general triaxial tension enforced on the model as in the case of axisymmetric loading. When $\alpha < 0.3$, the equivalent stress drops abruptly from its maximum point with little plastic strain, but soon after that this equivalent stress keeps raising up. This indicates that the plane strain behaviour is very sensitive to the triaxial stress state. Computed results also show that a larger initial void size, such as the $r = 0.25$ curves in broken line, can substantially alleviate the triaxial tension. This implies that at the time of attaining the same porosity the two material models ($r = 0.15$ and $r = 0.25$) can have quite different macroscopic stress/strain responses. That is to say, the void growth history must have a strong influence on the stress state; especially on the mean stress.

Figure 3 shows the increase of the void volume fraction vs the overall equivalent strain. The broken lines represent the parts contributed by the primary voids whilst the solid lines are those of the total parts. Naturally, the difference comes from the nucleation and growth of secondary voids. In each case the development of secondary voids at first accelerates the growth of the primary ones, or, alternatively, we may also say that a faster growth of the primary void favours the multiplication of secondary ones. However at the final stage the growth of the primary void may be suppressed owing to its coalescence with the secondary voids or to the too rapid development of the latter ones, as shown by the drop of the broken lines. It is easy to see that, among the three loading conditions, the plane strain case is the most favourable condition for void growth. This limits the maximum ductility that can be obtained in this case. Another interesting point in Fig. 3(c) is the approximately linear feature of most parts of the curves. This is in contrast with the exponential trend shown in Fig. 3(a) and 3(b).

The internal cracking condition of some typical cases are demonstrated in Fig. 4(a) at a level of being totally voided with a volume fraction f_v around 10%. The primary void changes its shape from an originally spherical type to an ellipsoidal one with its long axis parallel to the main loading direction, when the value of α tends to 0.49 as in the figure. At the same time the ductility of the material also increases enormously. It is interesting to notice the difference in damage feature and fractography at rupture. When the ductility becomes larger, the sites of secondary voids become scattered and the shape of these voids may be distorted in extreme cases to a thin slot. On the other hand in the case of, say, $\alpha = 0.35$ the site of secondary voids is more or less limited within a plane layer perpendicular to the main loading line. In the same figure we use broken lines to sketch out the regions that could be damaged by secondary voids at the final stage of rupture with a total void volume fraction f_v around 25%. It was not possible to proceed with the computation for $\alpha = 0.49$ to such an extension as even with $f_v = 10\%$ the elements were already very much elongated to thin triangles. It should also be noticed that in this case the secondary voids have totally encircled

and coalesced with the primary one, therefore it would be very difficult, if not impossible, to distinguish the original border line between them. The fact that the void growth measured in the tests of [14] and [17] is much higher than the theoretical prediction [2] can be explained as mainly caused by this coalescence mechanism, besides possibly the interaction effect that was neglected in the theoretical analysis. The wide spread of secondary voids in the case of $\alpha = 0.47$ and the long pulled shape of voids when $\alpha = 0.49$ are quite in accordance with the observations of the tests of axisymmetric bars, such as reported by Sun *et al.* [14], Xia *et al.* [15] and Sun and François [16].

Since the mean stress is low in the plane stress type of loading, the nucleation of secondary voids

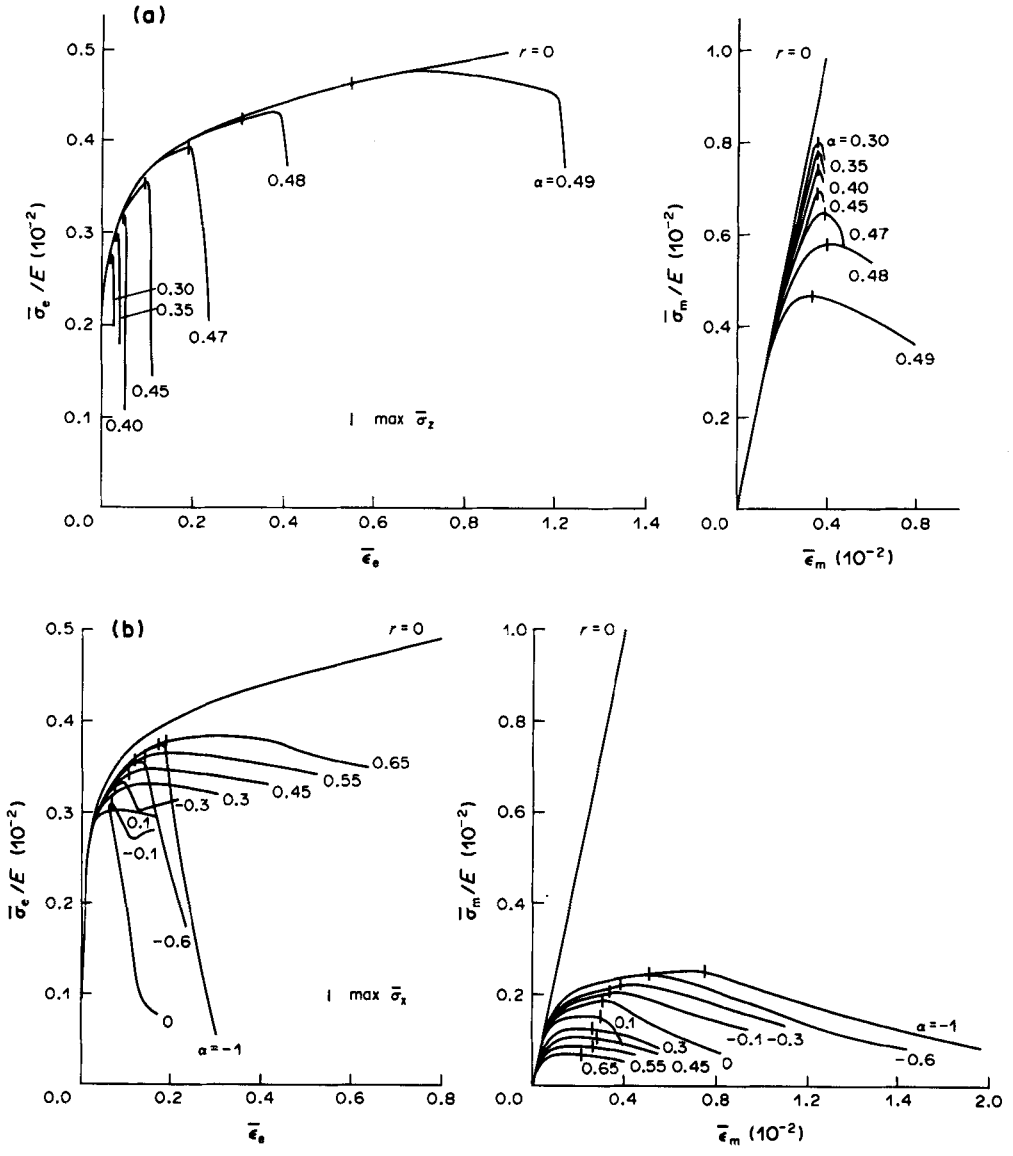

Fig. 2. *Caption on facing page.*

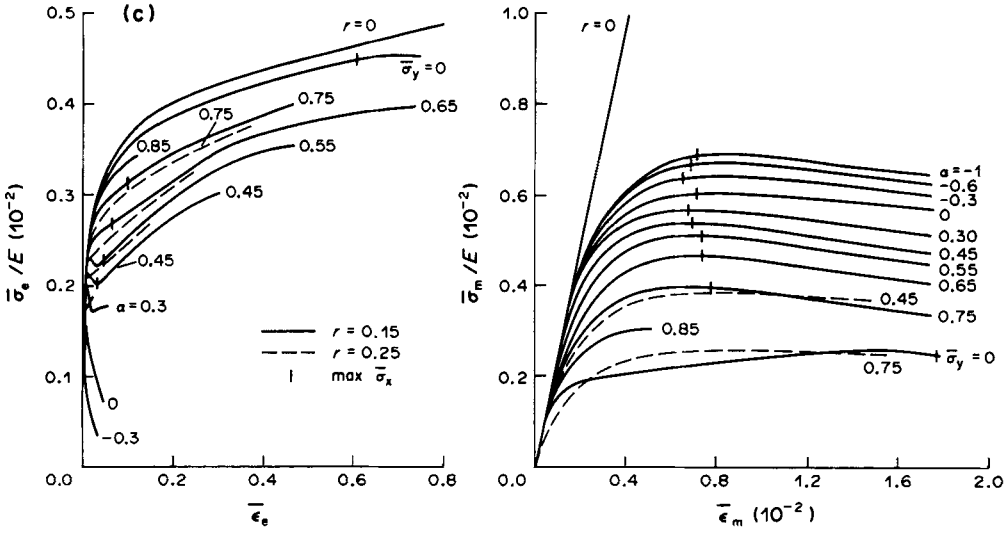

Fig. 2. The macroscopic equivalent stress–strain curves and the macroscopic mean stress–strain curves. (a) Axisymmetric models with spherical voids ($r = 0.15$). (b) Plane stress models with cylindrical voids ($r = 0.15$). (c) Plane strain models with cylindrical voids ($r = 0.15$, 0.25).

is found to be mainly governed by the strain criterion (7). The high strained region as shown in Fig. 4(b) is rather localized in a band perpendicular to the major principal stress direction.

Following this line cracking always starts at the vicinity of primary voids and protrudes from there into the material straightforwardly up to it crossing through the cell and meeting with the boundary with almost no zig-zag path in the middle way. Final rupture may occur approximately at a porosity of $f_v = 22\%$. In no case in plane stress loading does the damage mainly occur away from primary voids as seen in the other loading conditions.

In Fig. 4(c) is shown that the damage may occur from both parts which are near to or far from the primary void at higher triaxial stress level, e.g. $\alpha = -1$ to 0. However, when the triaxial stress is lowered down, the nucleation and growth of secondary voids mainly occurs around the primary void as shown for example by the case with $\alpha = 0.45$. As straining is carrying on, the final fracture could take place in the biaxial case with a flat faced crack perpendicular to the principal stress direction, but the cracked face might become fibrous as shown by the broken lines in Fig. 4(c) at $f = 22\%$ for the lower triaxial condition.

4. THE EFFECTS OF VOID SHAPE AND VOID GROWTH HISTORY AND COMPARISONS WITH THE WORKS OF PREVIOUS AUTHORS

Some further examples in the plane strain condition will be shown in this section to prove the effects of void shape and void growth history. One is implemented by considering a flat shape void as shown in Fig. 1(b) which has the same initial void volume fraction as the cylindrical void of $r = 0.15$, whereas another scheme is employing a larger initial cylindrical void of $r = 0.25$. Comparison of the mechanical behaviour of voided materials with different initial void volumes at some same stage of total porosity will then show the influence of void growth history on material behaviour. Both cases are subjected to plane strain loading. According to the definition in (2) the

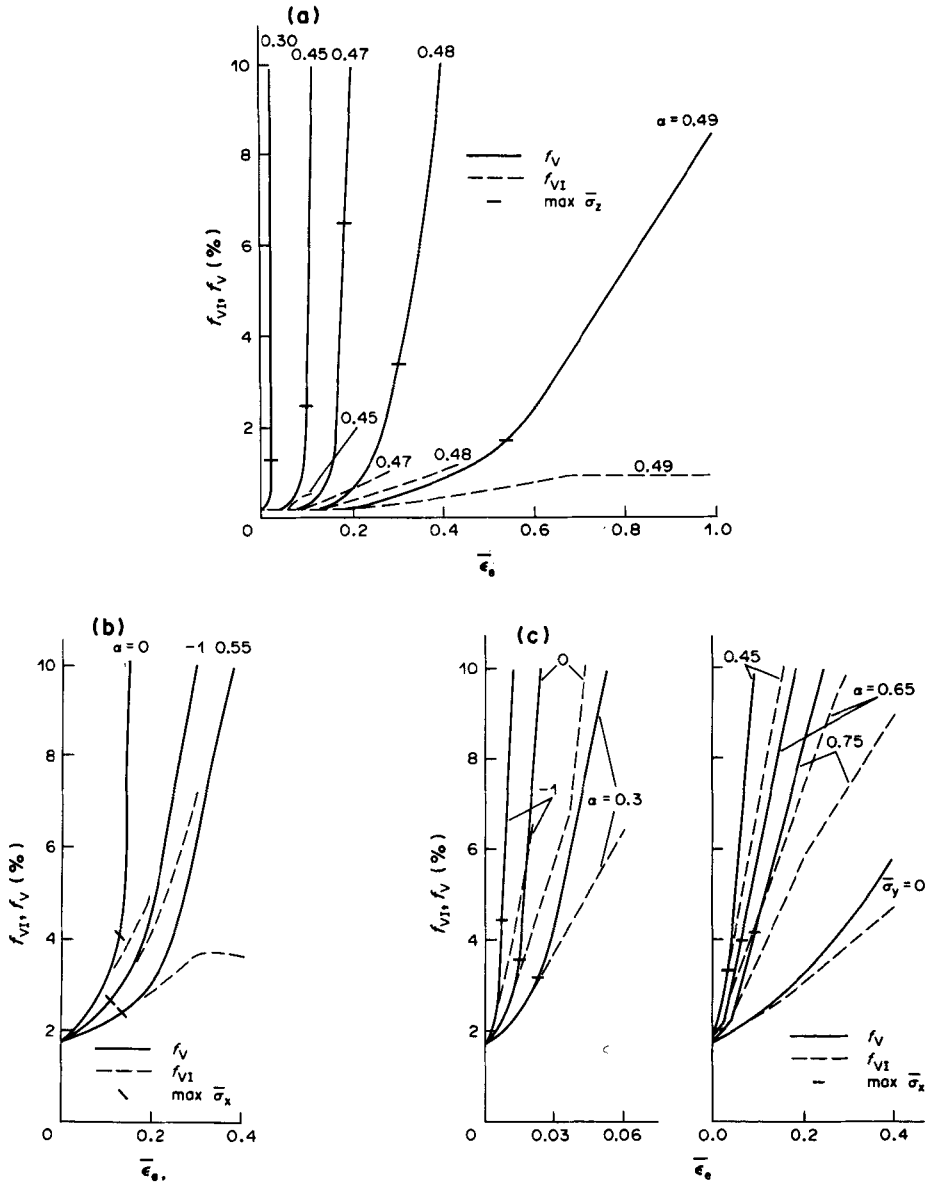

Fig. 3. The growth of void volume fraction vs equivalent strain (— total volume fraction f_v, --- volume fraction of primary voids f_{vi}). (a) Axisymmetric condition ($r = 0.15$). (b) Plane stress condition ($r = 0.15$). (c) Plane strain condition ($r = 0.15$).

flat void has an initial radius ratio $r = 0.40$, which retains the initial porosity of $f_{v0} = 1.76\%$, the same as that of the cylindrical void of $r = 0.15$ but has its void shape completely changed. The size of the mesh is such that the strong concentrations at the corners of the flat void are smoothed out. The larger void sample of $r = 0.25$ results in $f_{v0} = 4.90\%$ which is more than twice the value of the smaller one with $f_{v0} = 1.76\%$. These two samples will be compared at the total porosity of $f_v = 10\%$.

Computed results have been obtained for both the model A which has a flat void and the model with a cylindrical void of $r = 0.25$ under proportional straining conditions of $\alpha = -0.3, 0, 0.3, 0.45, 0.55, 0.65$ and 0.75. A huge decrease of mean stress response is observed in Fig. 2(c) for a larger initial void. Figure 5 collects together the results from the five models we have considered. Each point refers to a certain model under a certain mode of straining. The solid circles (for cylindrical void model with $r = 0.25$) and the inverted solid triangles (for flat void) together with the data obtained from previous computations exhibit a wide extent of stress–strain variation caused by the differences in loading condition, void shape and void growth history, when compared at the same porosity of $f_v = 10\%$. If it were reasonable to take these effects as negligible the distribution of the data would be rather compacted into a certain band-like curve for $\bar{\varepsilon}_e$ vs T. However, it is not the case in here. This advises us to handle carefully each material case, that is to be treated, by selecting an appropriate model that can really be taken as representative of its physical background.

Based on approximate rigid–perfectly plastic computations for special void geometries, Gurson [3] proposed approximate yield surfaces for void-containing materials. His formulae are now commonly adapted into the strain-hardening case by stating

$$\Phi = \left(\frac{\bar{\sigma}_e}{\sigma_{fl}}\right)^2 + 2f_v \operatorname{ch}\left(\frac{3\bar{\sigma}_m}{2\sigma_{fl}}\right) - (1 + f_v^2) = 0 \tag{8}$$

for a spherical void embedded in a spherically symmetric model, and

$$\Phi = (1 + 3f_v + 24f_v^6)^2 \left(\frac{\bar{\sigma}_e}{\sigma_{fl}}\right)^2 + 2f_v \operatorname{ch}\left(\sqrt{3}\,\frac{\bar{\sigma}_m}{\sigma_{fl}}\right) - (1 + f_v^2) = 0 \tag{9}$$

for a cylindrical void in the plane strain condition. These plastic potentials are formulated in terms of the macroscopic equivalent stress $\bar{\sigma}_e$ and of the macroscopic mean stress $\bar{\sigma}_m$ both normalized by the current flow stress σ_{fl} of an unvoided continuum. The value of this flow stress is depending on the overall equivalent strain $\bar{\varepsilon}_e$ that has been attained. In large strain calculations the difference between the plastic part and the total part of equivalent strain can be neglected. The parameter f_v in (8) and (9) as usual represents the porosity.

Tvergaard [7–8] modified Gurson's model by suggesting that some additional and adjustable parameters be added into the form given by (8). He took the yield surface as

$$\Phi = \left(\frac{\bar{\sigma}_e}{\sigma_{fl}}\right)^2 + 2f_v q_1 \operatorname{ch}\left(q_2 \frac{3\bar{\sigma}_m}{2\sigma_{fl}}\right) - (1 + q_3 f_v^2) = 0. \tag{10}$$

If $q_1 = q_2 = q_3 = 1$, (10) coincides with (8). Tvergaard proposed to use $q_1 = 1.5$, $q_2 = 1$ and $q_3 = q_1$, in order to improve the predictions of the critical strain for localization into a shear band.

Recently Guennouni and François [4, 5] have made use of finite element analysis on a plane strain square cell which is also made of rigid–perfectly plastic material surrounding a cylindrical void. Along the square boundaries, either pure normal stresses or together with shear stress are enforced to simulate different overall triaxiality stress states. The porosity condition can be changed by assigning different void size as in Gurson [3]. The new yield surface proposed by Guennouni and François can be written as

$$\Phi = \sqrt{3}\left[\left(\frac{\bar{\sigma}_e}{B\sigma_{fl}}\right)^2 + \left(\frac{\bar{\sigma}_m}{A\sigma_{fl}}\right)^2\right]^{1/2} = 1 \tag{11}$$

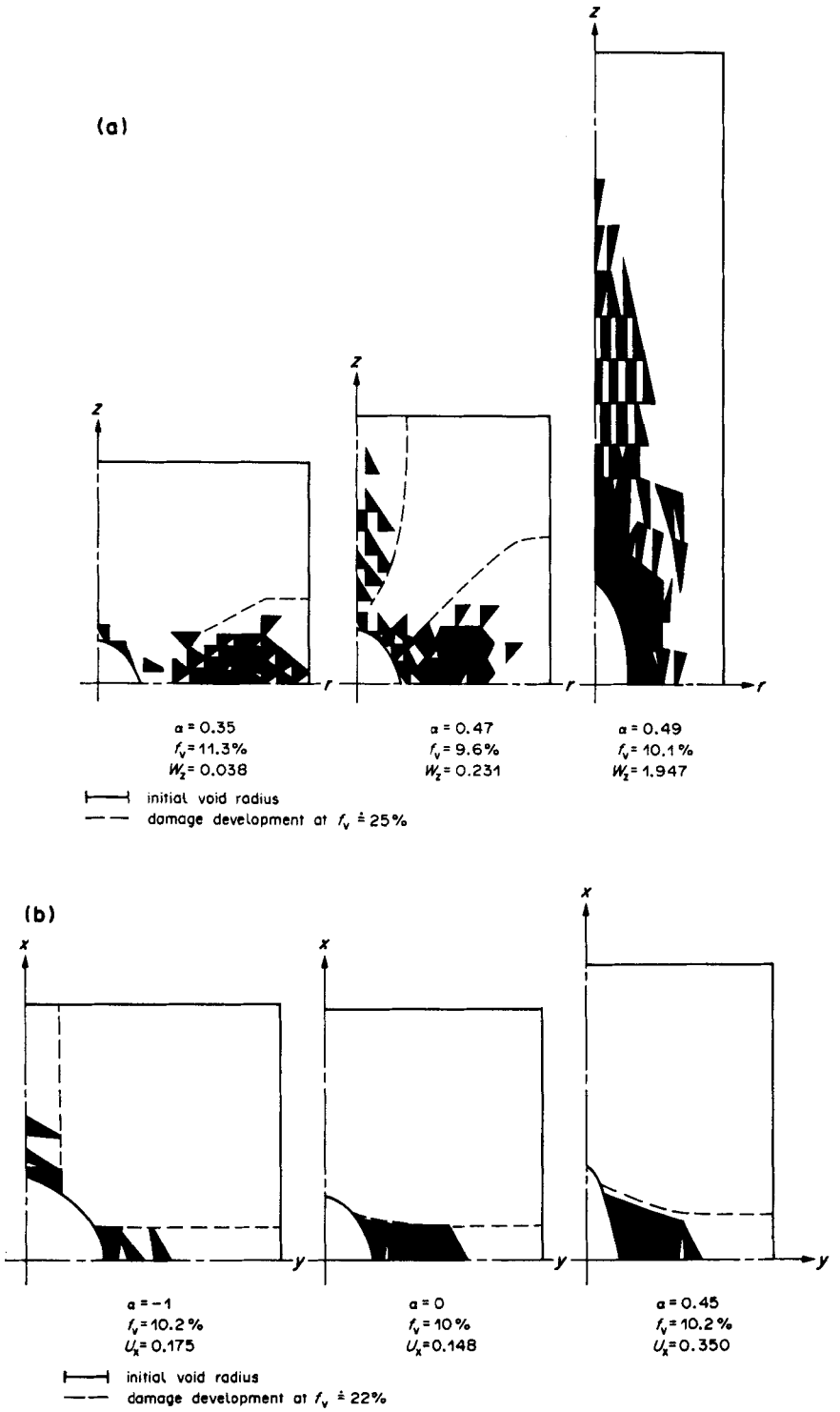

Fig. 4. *Caption on facing page.*

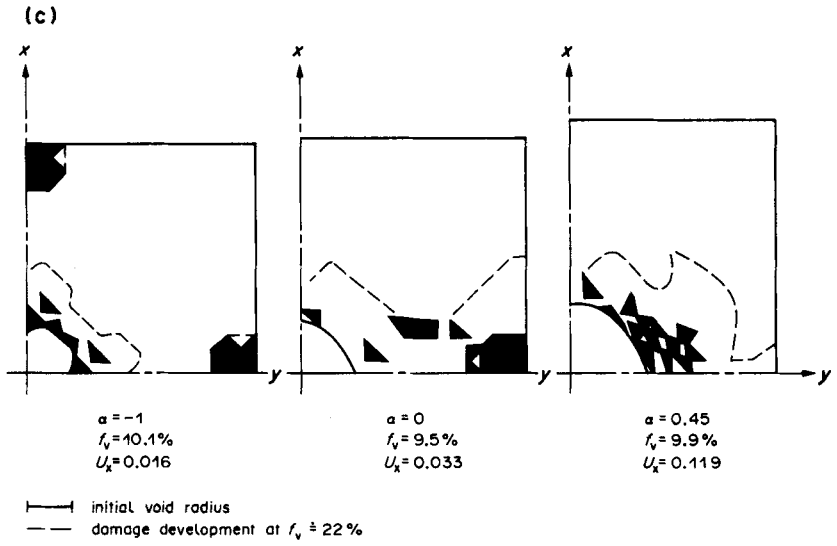

Fig. 4. Illustration of the damage development. (a) Axisymmetric models ($r = 0.15$). (b) Plane stress models ($r = 0.15$). (c) Plane strain models ($r = 0.15$).

where

$$A = -(1 - 1.92f_v + 5.57f_v^2 - 6.04f_v^3)\ln f_v$$

$$B = \begin{cases} \sqrt{3}(1 - 1.33f_v^{0.6}) & \text{when } f_v < 0.1256 \\ 2.06\,[\exp(-4.9f_v) - 4.4\,10^{-2}] \end{cases}$$

otherwise and σ_{fl} is the current flow stress as before.

Comparison of the plastic loading condition between the present results of numerical calculations and those of Gurson, Tvergaard and Guennouni and François are shown in Figs 6 and 7 at the total porosity of $f_v = 3\%$ and of $f_v = 10\%$, respectively. Each of the data is representing a certain model subjected to a certain mode of straining. It is not possible to have the data of the plane strain

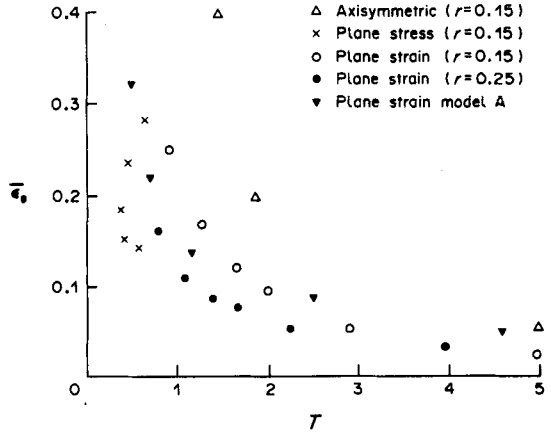

Fig. 5. Comparison between the plastic loading points at $f_v = 10\%$ for different models.

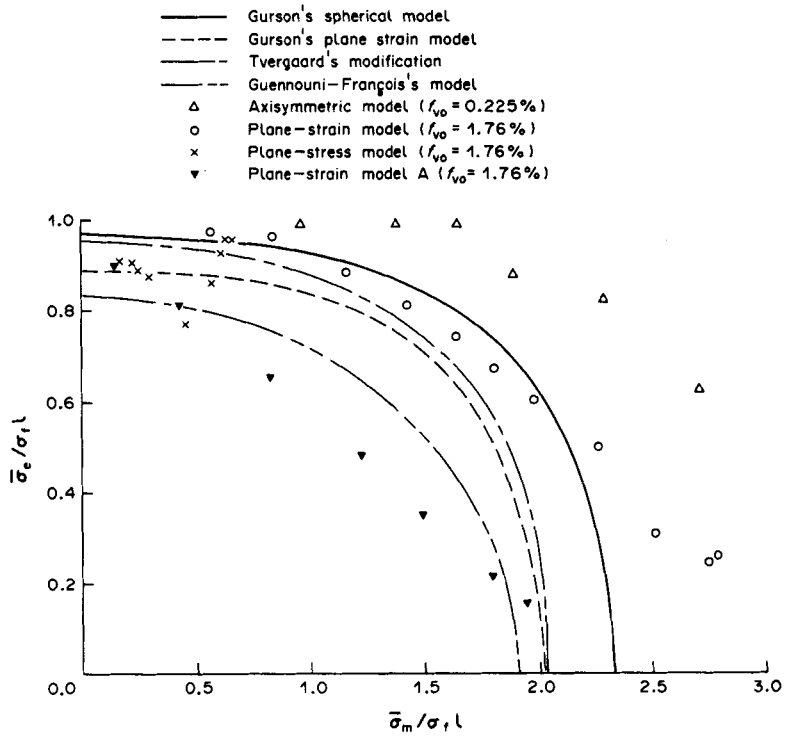

Fig. 6. Comparison between the plastic loading points for different models at $f_v = 3\%$.

model with $r = 0.25$ shown in Fig. 6, since this model starts with an initial void volume fraction that is larger than 3%. The difference shown by the plane strain models in blank circles, solid circles and inverted solid triangles in these figures indicate the strong effects cause by void growth history and void shape on the plastic loading stress state. The data represented by blank triangles and crosses are referring to the spherical void in axisymmetric loading and the plane stress void model, respectively. The plane strain data for spherical voids are more or less included between these two loading cases. Usually the axisymmetric void model yields rather scattered results in these figures. This is because it has the smallest primary void volume fraction; then the secondary void makes the larger contribution to the total porosity. Even with the equal sized elements chosen for the mesh of numerical calculations, when secondary voids initiate at sites far from the central axis of the model, a large amount of void volume may suddenly appear and could cause an abrupt change in the macroscopic response. This is also the reason why a larger scatter is seen in Fig. 7 at $f_v = 10\%$ than in Fig. 6 at $f_v = 3\%$. It might not be unreasonable if we notice the usual scattering feature of the data recorded in experiments concerning the microstructural behaviour at the stage of serious damage. The stress response yielded by the axisymmetric model is considerably higher than that of Gurson or Tvergaard. This can be attributed to the elasticity effect that is neglected by using a "rigid" assumption in Gurson's model. A similar situation can also be seen in the Fig. 4 of Tvergaard's study [8] on materials containing spherical voids.

A further comparison between the present computations and the formulae given by Rice and Tracey [2] and by Guennouni and François [4] is made for estimating void growth. Only a single

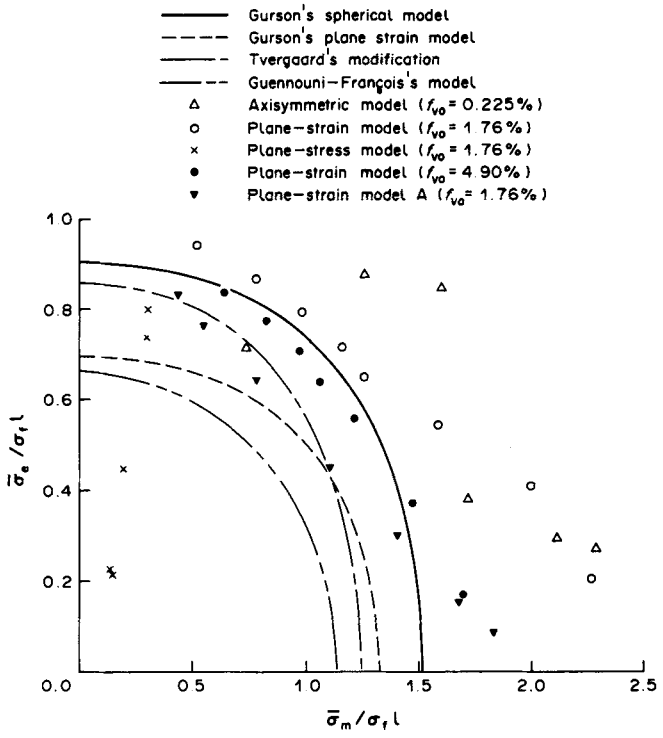

Fig. 7. Comparison between the plastic loading points for different models at $f_v = 10\%$.

void is accounted for in the previous models; therefore the formulae can be written as

$$\frac{\dot{f}_{v1}}{f_{v1}} = \frac{3\dot{a}}{a} = 0.849\,\dot{\bar{\epsilon}}_e \exp\left(\frac{3\bar{\sigma}_m}{2\bar{\sigma}_e}\right) \tag{12}$$

based on the Rice–Tracey model with a single spherical void embedded in an infinite medium, and

$$\frac{\dot{f}_{v1}}{f_{v1}(1-f_{v1})} = \left(\frac{B}{A}\right)^2 \dot{\bar{\epsilon}}_e \left(\frac{\bar{\sigma}_m}{\bar{\sigma}_e}\right) \tag{13}$$

according to the plane strain model of Guennouni–François in the case of strain-hardening material, where

$$A = \beta\{1 + [3(p-1) - 0.77p^2]f_{v1}\}$$

$$B = \sqrt{3}\left[1 - \left(2.45 - \frac{0.368}{\sqrt{p-0.892}}\right) f_{v1}^{0.6(1+\sqrt{p-1})}\right]$$

$$\beta = \left[\frac{f_{v1}^{(1-p)} - 1}{p-1}\right]^{1/p} \qquad p = 1 + n$$

and n is the strain hardening exponent in (5) which has been taken to be 0.15 here in this paper. Making use of the macroscopic stresses $\bar{\sigma}_e$ and $\bar{\sigma}_m$ and the macroscopic increment $\dot{\bar{\epsilon}}_e$ of equivalent strain obtained at the end of each increment of generalized time, we are able to calculate the corresponding increment $\dot{f}_{v1}$ of the void volume fraction predicted by (12) and (13). An integration

Table 1. Comparison between f_{vl} and f_{RT} in axisymmetric loading ($r = 0.15$)

f_v	α / f_{vl}	0.30	0.35	0.40	0.45	0.47	0.48	0.49
0.5%	f_{vl}(%)	0.316	0.326	0.336	0.352	0.39	0.336	0.366
	f_{RT}(%)	0.319	0.323	0.330	0.345	0.336	0.343	0.418
1.3%	f_{vl}(%)	0.328	0.336	0.355	0.409	0.477	0.547	0.619
	f_{RT}(%)	0.337	0.336	0.352	0.406	0.482	0.579	0.811
4.5%	f_{vl}(%)	0.341	0.357	0.388	0.463	0.580	0.773	0.859
	f_{RT}(%)	2.101	4.070	0.898	0.484	0.601	0.887	1.749

of all these increments accumulated up to a certain time gives the total value of void volume fraction at that time.

Table 1 and Table 2 present the comparisons between our numerical calculations and those integrated from the formulae of Rice and Tracey and Guennouni and François, respectively. For the axisymmetric case with a spherical void comparisons are made at three stages of total voiding, which are $f_v = 0.5$, 1.3 and 4.5%, as given in Table 1. Usually the void volume fraction f_{RT} given by (12) is much smaller than the total value f_v attained by our computer simulation. However the results of f_{RT} are in rather good accordance with those values of the volume fraction f_{vl} of primary void, until around a total porosity of $f_v = 4.5\%$. Sooner or later afterwards the result of Rice–Tracey formula will quickly tend to infinity, owing to the relatively rapid drop of the macroscopic equivalent stress $\bar{\sigma}_e$ with respect to the macroscopic mean stress $\bar{\sigma}_m$; which makes the exponential part in the formula (12) multiply enormously. The large discrepancies between f_{vl} and f_{RT} in the cases of $\alpha = 0.3$, 0.35, 0.40 and 0.49 in Table 1 are reflecting the starting of this critical stage. Table 2 shows the good agreement between the void volume fraction f_{GF} of Guennouni–François formula (13) and the present numerical calculations for primary void at different stages of porosity ($f_v = 3$, 10 and 20%) which actually cover the whole loading history. However the value of f_{GF} is still much smaller than the total value of f_v. It needs to be noticed that by using the macroscopic responses obtained from the numerical calculations, the interaction effect between two generations of voids are introduced into the integration results of [12] and [13], although the derivation of these formulas is based on single voids.

5. CONCLUSIONS

During the process of ductile damage caused by void growth the interaction between two generations of voids is, in effect, shown throughout this paper to play a very important role which has not yet been fully recognized. In no respect can the real internal voiding condition be correctly represented by simple modelling based on a single void analysis. As has been pointed out by

Table 2. Comparison between f_{vl} and f_{GF} in plane strain loading ($r = 0.15$)

f_v	α / f_{vl}	−1	−0.6	−0.3	0	0.45	0.55	0.65	0.75
3%	f_{vl}(%)	2.65	2.71	2.93	2.90	2.86	2.80	2.61	2.61
	f_{GF}(%)	2.21	2.25	2.31	2.31	2.53	2.55	2.46	2.54
10%	f_{vl}(%)	3.64	4.00	4.71	4.49	7.22	6.82	6.79	6.48
	f_{GF}(%)	3.29	3.42	3.72	3.15	5.59	6.04	6.54	7.10
20%	f_{vl}(%)	5.83	6.57	8.95	7.47	10.90	10.40	11.26	10.68
	f_{GF}(%)	7.47	6.55	7.25	4.72	9.23	10.18	11.42	12.75

Guennouni and François [5] this effect is not additive, or in other words, the macroscopic response of a medium with one order of voids is not equivalent to another that has the same void volume fraction but composed of two orders of voids.

The interaction effect is much more complicated through the strong influence of loading conditions (axisymmetric, plane stress and plane strain etc.), of initial void shape (spherical, cylindrical and flat, etc.) and of void growth history (larger or smaller initial porosity). Special care should therefore be taken in selecting an appropriate constitutive characterization for porous materials. A plastic potential does not seem to exist when damage is accumulated to a large extent. Generally speaking, a single internal variable based on void volume fraction is not sufficient for theoretical descriptions of the damage in porous materials.

Lastly but not the least, there are still some effects that may have a substantial influence, which however, are not accounted for up to now. Such as the non-proportionality of straining in actual loading, the existence of other microstructural features that have not yet been investigated. Theoretical modelling does help us to understand the microstructural mechanism, the damage evolution and the characterizing parameters that should be chosen to describe the process of ductile damage. However, for the sake of making a quantitative estimation of its macroscopic/microscopic behaviour, the undetermined effects involved in physical material should be completed and taken into account by employing experimental results.

Acknowledgements—This study was arranged and supported by an agreement between the CNRS and the Academia Sinica. The first-named author wishes to express his special thankfulness to the CNRS for providing the financial support for him during his visit in France.

REFERENCES

1. McClintock F. A. (1968) A criterion for ductile fracture by the growth of holes. *J.A.M.* **35,** 363–371.
2. Rice J. R. and Tracey D. M. (1969) On the ductile enlargement of voids in triaxial stress fields. *J. Mech. Phys. Solids* **17,** 201–217.
3. Gurson A. L. (1977) Continuum theory of ductile rupture by void nucleation and growth: part I—Yield criteria and flow rules for porous ductile media. *J. Engng Mater. Tech.* **99,** 2–15.
4. Guennouni T. and François D. (1987) Constitutive equations for rigid plastic or viscoplastic materials containing voids. *Fatigue Fract. Engng Mater. Struct.* **10,** 399–418.
5. Guennouni T. and François D. (1987) Constitutive equations and cavity growth rate for a porous plastic medium, *Mechanical Behaviour of Materials*—V, *Proc. ICM5*, Beijing, China Vol. 1, pp. 155–160.
6. Yamamoto H. (1978) Conditions for shear localization in the ductile fracture of void-containing materials. *Int. J. Fract.* **14,** 347–365.
7. Tvergaard V. (1982) Ductile fracture by cavity nucleation between larger voids. *J. Mech. Phys. Solids* **30,** 265–286.
8. Tvergaard V. (1982) On localization in ductile materials containing spherical voids. *Int. J. Fract.* **18,** 237–252.
9. Needleman A. (1972) Void growth in an elastic–plastic medium. *J.A.M.* **39,** 964–970.
10. Li G. C. and Howard I. C. (1983) The effect of strain-softening in the matrix material during void growth. *J. Mech. Phys. Solids* **31,** 85–102.
11. Li G. C. and Howard I. C. (1983) The sensitivity of the macroscopic consequences of void growth in ductile materials to various mechanical and geometrical microparameters. *Int. J. Solids Struct.* **19,** 1089–1098.
12. Hancock J. W. and Mackenzie A. C. (1976) On the mechanisms of ductile failure in high-strength steels subjected to multiaxial stress states. *J. Mech. Phys. Solids* **24,** 147–169.
13. Lautridou J. C. and Pineau A. (1981) Crack initiation and stable crack growth resistance in A508 steels in relation to inclusion distribution. *Engng Fract. Mech.* **15,** 5–71.
14. Sun Y. Q., Detraux J. M., Touzot G. and François D. (1983) Mécanisme de la rupture ductile dans la fonte à graphite sphéroïdal ferritique. *Mem. Etudes scient. Rev. Metall.* **80,** 183–195.

15. Xia X. X., Yang G. Y., Hong Y. S. and Li G. C. (1987) Tests and analysis on the ductile fracture of axisymmetric specimens, *Mechanical Behaviour of Materials, V, Proc. ICM5*, Beijing, China, Vol. 1, pp. 199–204.
16. Sun Y. Q. and François D. (1984) Influence du taux de triaxialité de contraintes sur la coalescence des cavités et la morphologie des cupules de la fonte à graphite sphéroïdal, *Revue de Métallurgie CIT*, pp. 809–817.
17. Marini B., Mudry F. and Pineau A. (1985) Experimental Study of Cavity Growth in Ductile Rupture, *Engng Fract. Mech.* **22,** 989–996.
18. McMeeking R. M. and Rice J. R. (1975) Finite element formulations for problems of large elastic–plastic deformation. *Int. J. Solids Struct.* **11,** 601–615.